S L H C - P P

M I L E S T O N E   R E P O R T

EU MILESTONE: 7.1

Document identifier:	**SLHC-PP-M7.1-1002168-v1.0**
Contractual Date of Delivery to the EC:	**End of Month 14 (May 2009)**
Actual Date of Delivery to the EC:	**29/5/2009**
Document date:	**20/5/2009**
Milestone Title:	**List of required improvements for the design of the high duty factor plasma generator to function at 6% duty factor**
Work package:	**WP7: Development of critical components for the injectors**
Lead Beneficiary:	**CERN**
Authors:	**D.Faircloth, M.Kronberger, J.Lettry, C.M.Schmitzer, R.Scrivens**
Document status:	**Released**
Document link:	https://edms.cern.ch/document/1002168/1

History of Changes

Version	Date	Responsible	Modification
0.1	2009-05-20	M. Kronberger	Creation of document
1.0	2009-05-28	M. Kronberger	Corrections from co-authors implemented
2.0	2009-05-29	J. Lettry	Inserted chapter 6
2.1	2009-05-29	M. Kronberger	Final version

ABSTRACT

The full sLHC upgrade includes the Superconducting Proton Linac (SPL) delivering 5GeV H-ions to a new proton synchrotron (PS2). In addition, this SPL could be capable of high duty factor operation (of the order of a few percent) in order to create beams for new physics studies (including possible high intensity neutrino generation and radioactive ion beams). The major increase in repetition rate demands the replacement of the RF powered, non-cesiated H- source that will be operated at Linac4. The present report summarizes the technical improvements that are required for operation of the H- source at a duty factor of several percent.

1   INTRODUCTION

The improvements required to upgrade the plasma generator (PG) of the Desy-Linac4 H- source [1] to 50Hz operation at 6% duty factor are listed below:

- Active cooling of the plasma chamber, the extraction collar, the electron gun and the antenna.

- Replacement of materials used in the Linac4 source by materials with better heat conductivity (e.g. replacement of Al_2O_3 and Macor by AlN).

- Brazing of conductors on insulators to improve and control thermal contact properties.

- Modification of H_2 gas injection region.

- Protecting metallic source components, ferrites and permanent magnets from possible RF inductive heating.

The following sections provide an overview on the strategy chosen to address each of these improvements. Wherever necessary, illustrative examples of the assessment methods and of intermediate tests are provided.

2   ENGINEERING, SUB-ASSEMBLIES AND SCALING

To facilitate the development process, the PG has been split into four parts with different functionality (Fig. 1):

- The H_2 gas injection region, including the gas pipe, piezo valve support, the ignition element with its supporting structure, and the plasma chamber entry plate;

- The plasma chamber with the antenna, the magnets and ferrites and their supporting structures;

- The extraction region, including filter magnets, collar, and front plate;

- The mechanical support with the RF enclosure box.

Each of these parts will be designed separately in the development of the HP-SPL PG. The mechanical support includes an adapter to a DN-150 flange which allows mounting on a vacuum tank for test purposes. A confinement box encasing the PG will prevent RF noise.
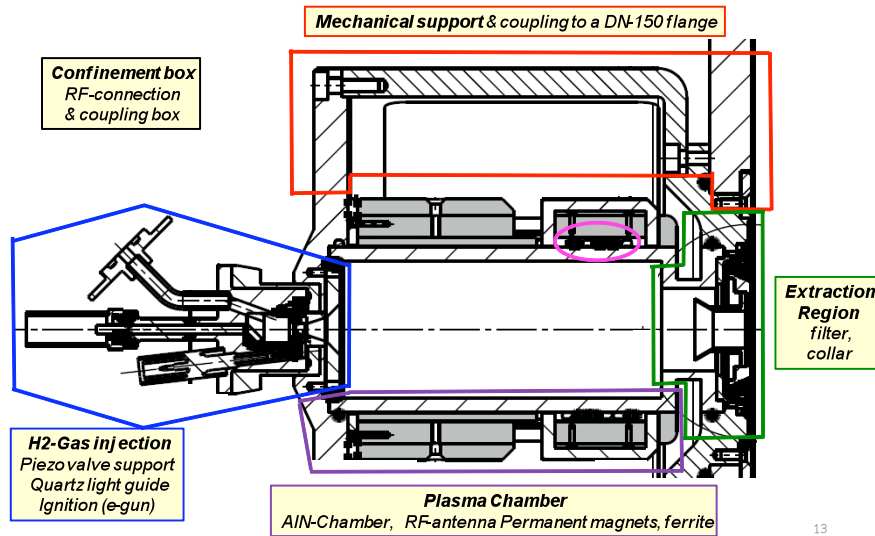
Figure 1: *Sub-assemblies of the HP-SPL plasma generator: H_2 gas injection region (blue), Plasma Chamber (purple), Extraction Region (green) and Confinement Box (red).*

The thermal properties of the PG will be modeled as a function of its internal volume. In order to define the optimum size, a parameterized CAD model is in preparation. This parameterized model includes three scaling parameters (Fig. 2): The inner diameter and length of the plasma chamber, and the length of the antenna coil. The parameterization improves the flexibility of the CAD model and allows for a fast production of PG models where one of the parameters is varied consecutively. The PG models will be used in various simulation tools, as e.g. ANSYS or Opera. In order to speed up the convergence of the simulations, any small structures with negligible impact on the outcome (e.g. screw holes, wires, etc.) are not exported while remaining available on a dedicated drawing layer.
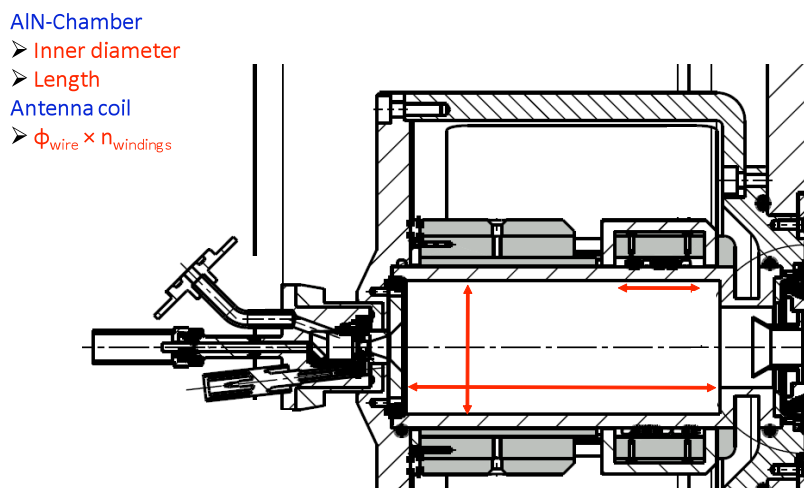

Figure 2: *Scaling parameters implemented in the CAD model of the HP-SPL plasma generator. The individual parameters are: plasma chamber inner diameter and length, and the length of the antenna coil.*

3   MATERIALS

The average power encountered by each sub-assembly is given in Table 1 for Linac4 (100 kW RF peak power, 0.08% duty factor) and HP-SPL (100kW peak RF power, 6% duty factor) [2,3].

sub-assembly	Average power [W]	
	Linac 4	HP-SPL
H_2 gas injection region	0.8	60
plasma chamber	65.5	4910
extraction region	13.7	1030
total	80	6000

Table 1: Average heat load encountered in Linac4 and HP-SPL by each sub-assembly. The heat load at the extraction region includes the heat load on the front part of the plasma chamber.

To improve the transport of heat away from surfaces and components that are in direct or indirect contact with the plasma, critical components made of low thermal conductivity materials may have to be exchanged with high thermal conductivity materials in the HP-SPL PG. This regards mostly the insulators used in the collar region and the electron gun and the ceramic plasma chamber, but also those components where the heat flux is limited by a small cross-section, for example the funnel electrode of the collar. In addition, an exchange of materials may be necessary at positions where welding is used for thermal contact optimization. Table 2 provides a summary of thermally critical components and possible material alternatives, together with their thermal conductivities k at room temperature.

Sub-assembly	Component	Material Linac4	Thermal conductivity k [W/mK]	Material SPL (proposed)	Thermal conductivity k [W/mK]
plasma chamber	plasma chamber	Al_2O_3	35	AlN	170
	Aperture disk	Macor	1.45	AlN	170
electron gun	Insulation disk	Macor	1.45	AlN	170
extraction region	Insulation body	Macor	1.45	AlN	170
	Funnel electrode	SS316	13.9	Molybdenum	141
				Tungsten	163
				Titanium	24
	Mica insulation	Mica	0.5	AlN	170

Table 2: Critical components, as identified in [3], and possible material alternatives in the HP-SPL plasma generator.

4   COOLING SYSTEMS

Specific cooling systems are necessary to keep temperatures and thermal stresses in each sub-assembly within material specifications. In the following, the cooling strategies for each sub-assembly are described. Table 3 summarizes the preliminary parameters of all cooling circuits discussed in the text. All cooling circuits will be operated with demineralized water (c_p = 4.181J/kgK; viscosity μ = $1.002 \cdot 10^{-3}$kg/ms; k = 0.58W/mK). The necessary flow rates have been estimated from the time average heat flow per sub-assembly. In the calculations of the pressure drop Δp of the cooling circuits, a minimum return pressure of 2 bars has been assumed. All numbers have been calculated with a simple model and will be validated by computational fluid dynamics (CFD) simulations. The cooling circuits will be designed for the maximum pressure plus an overpressure safety margin of 2 bars to minimize the risk of leakage.

Sub-assembly / component	Cooling option	Heat flow [W]	ΔT [K]	Water flow [l/min]	Circuit cross section [cm²]	Flow velocity [m/s]	Δp [bar]	Reynolds number	Heat transfer coefficient [W/m²K]	In-Out
H₂ gas injection		60	30	0.03	0.3 x 0.3	0.07	<0.1	210	700	
Plasma Chamber	Race track	4910	30	2.4	1.5 x 0.3	0.9	0.2	4500	5000	R / R
	Parallel	4910	30	2.4	1.5 x 0.3	0.9	0.1	4500	5000	F / R
	Helicoidal	4910	30	2.4	1.0 x 0.3	1.3	0.4	6000	6700	F / R
Antenna		?	30	?	0.3 x 0.3	?	?			
Extraction region		1030	30	0.5	0.3 x 0.3	1.2	<0.1	3500	6700	

Table 3: Cooling system nominal parameters (only indicative values). The last column (in-out) indicates the position of water injection extraction for the different options for the plasma chamber cooling (F = front, R = rear).

4.1   H₂ GAS INJECTION REGION

The H₂ gas injection region will be an adapted version of the new DESY H⁻ ignition source design with removed optical port and gas injection and electrical connector shifted towards the middle. The new cathode is rotational symmetric in the new design, with the opening of the gas line at the top and a spherical inner surface. The shapes of the insulators have been slightly modified for improved mechanical stability. The copper wire supplying the anode with a voltage of several 100 Volts will be insulated to avoid sparking between the wire and the stainless steel body of the ignition element. Due to the comparably low heat load encountered for this sub-assembly (1% of the total heat load), the very basic cooling circuit consists of two copper tubes with rectangular cross section soldered onto the ignition element body.

4.2 PLASMA CHAMBER

The plasma chamber receives more than 85% of the total power radiated by the plasma. Therefore, a sophisticated cooling strategy is required to keep temperatures and thermal stresses within material specifications. To optimize heat transportation through the chamber wall, the chamber will be made of. A cylindrical polycarbonate sleeve with engraved cooling channels is put around the plasma chamber. The coolant will be in direct contact with the surface of the plasma chamber to optimize heat dissipation. O-rings placed at both ends of the cooling sleeve will ensure leak tightness of the circuit.
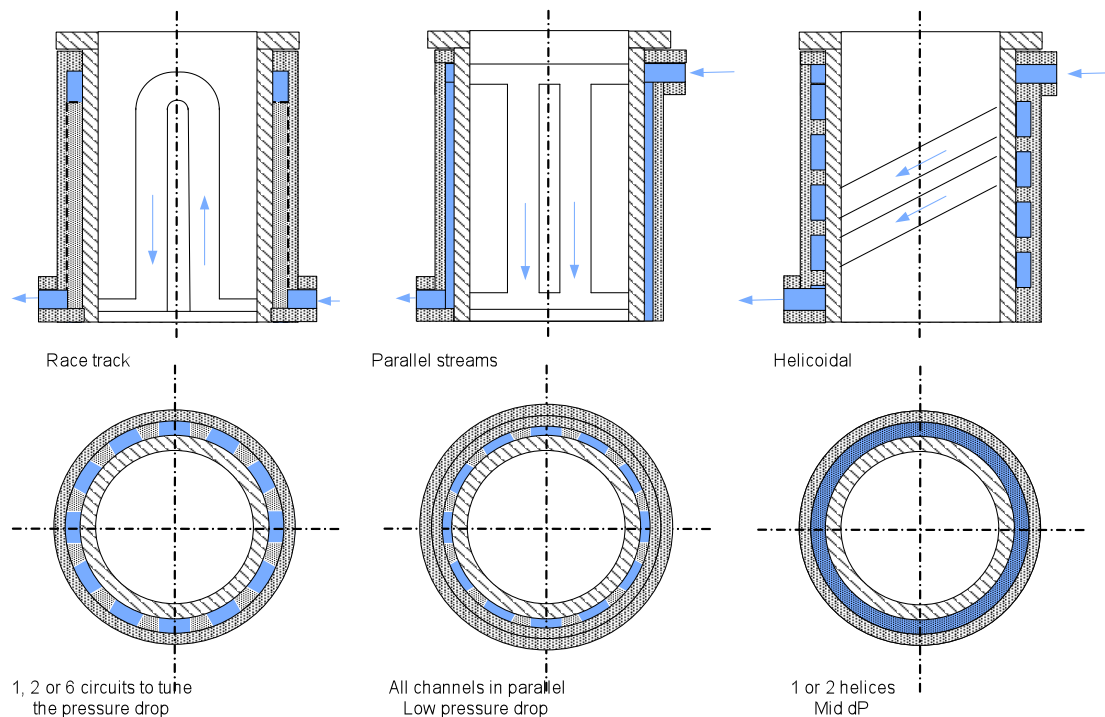

Figure 3: *Schematic view of possible cooling circuit layouts of the AlN-plasma chamber. The flow directions are indicated.*

Fig. 3 shows the three proposed designs of the plasma chamber cooling circuit that are mentioned in Table 3. To remove 4.9kW with an increase of the coolant temperature T of less than 30K, a minimum flow rate of 2.4l/min is required. The circuit cross section for the parallel and race track cooling circuits has been calculated for a plasma chamber with 58mm outer diameter and for eight parallel channels that cover a total 2/3 of the outer surface of the plasma chamber. In the case of the helicoidal cooling circuit, a helix with eight windings has been assumed. The pressure drop Δp has been calculated for a length of the cooled plasma chamber section of 120mm.

4.3 EXTRACTION REGION

Heat transportation in the collar may be improved a) by using AlN for all insulating component, and b) by brazing together conductors and insulators. Possible material combinations have been discussed with experts and brazing tests are deemed necessary.

No final decision has been taken yet on the position and design of the cooling circuit; the Reynolds number and the pressure drop Δp quoted in Table 3 are for a cooling circuit with inner diameter = 3mm and length = 500mm, and for a flow rate to 0.5l/min.

4.4 ANTENNA

A water-cooled hollow tube antenna made of copper will be used in the SPL H⁻ plasma generator to dissipate the heat produced by ohmic heating. The dimensions of the antenna will be comparable to the antenna used at the ORNL Spallation Neutron Source (SNS), which has an inner diameter of 3mm [4].

5 MECHANICAL STABILITY OF THE AIN PLASMA CHAMBER

The mechanical stability of the AIN plasma chamber under operation has been assessed by a finite element model of the chamber. To simplify calculations, only a cylindrical section of the plasma chamber with l = 150mm, d_{inner} = 48mm and d_{outer} = 58mm was considered. All three cooling scenarios presented before have been addressed in different simulations. The cooling circuits were imprinted onto the chamber wall to simulate the flow of a coolant. The heat transfer coefficient between AIN and coolant was set to values between 8000 and 10000 W/m²K. The total stress experienced by the plasma chamber was assumed to be due to two processes:

- Thermal stresses due to temperature gradients inside the chamber

- Mechanical stresses due to evacuation and coolant pressure

Simulating the mechanical stresses was achieved by dividing the plasma chamber into three regions that experience different pressures P:

- unevacuated region (P = 0 bar): outside vacuum o-rings

- Evacuated region (P = 1 bar): inside vacuum o-rings, no coolant pressure

- Evacuated + coolant flow (P = 5 + 1 bar): inside vacuum o-rings, pressure from coolant.

The coolant pressure was assumed to be 5bars, what corresponds to the maximum pressure expected in our system.

Thermal stresses were introduced by modelling the temperature distribution inside the plasma chamber. The heat load from the plasma was distributed according to the results presented in [3]. The total heat load was set to 6kW to simulate the worst case in HP-SPL. The mechanical support of the chamber was simulated by a frictionless support with free movement perpendicular to the cylinder axis at each end of the plasma chamber. As in the real case, this setting allowed for unrestricted thermal expansion in radial direction but suppressed thermal expansion in axial direction.

The results of the calculations are shown in Figs. 4a to 4c. In all three cases, the maximum thermal stresses experienced by the AIN plasma chamber are below 100MPa, which is by a factor two lower than the maximum stress allowed for this material (200MPa). The largest stresses are observed at the inside of the plasma chamber, at the position of the heat load maximum.

a)

b)

c)
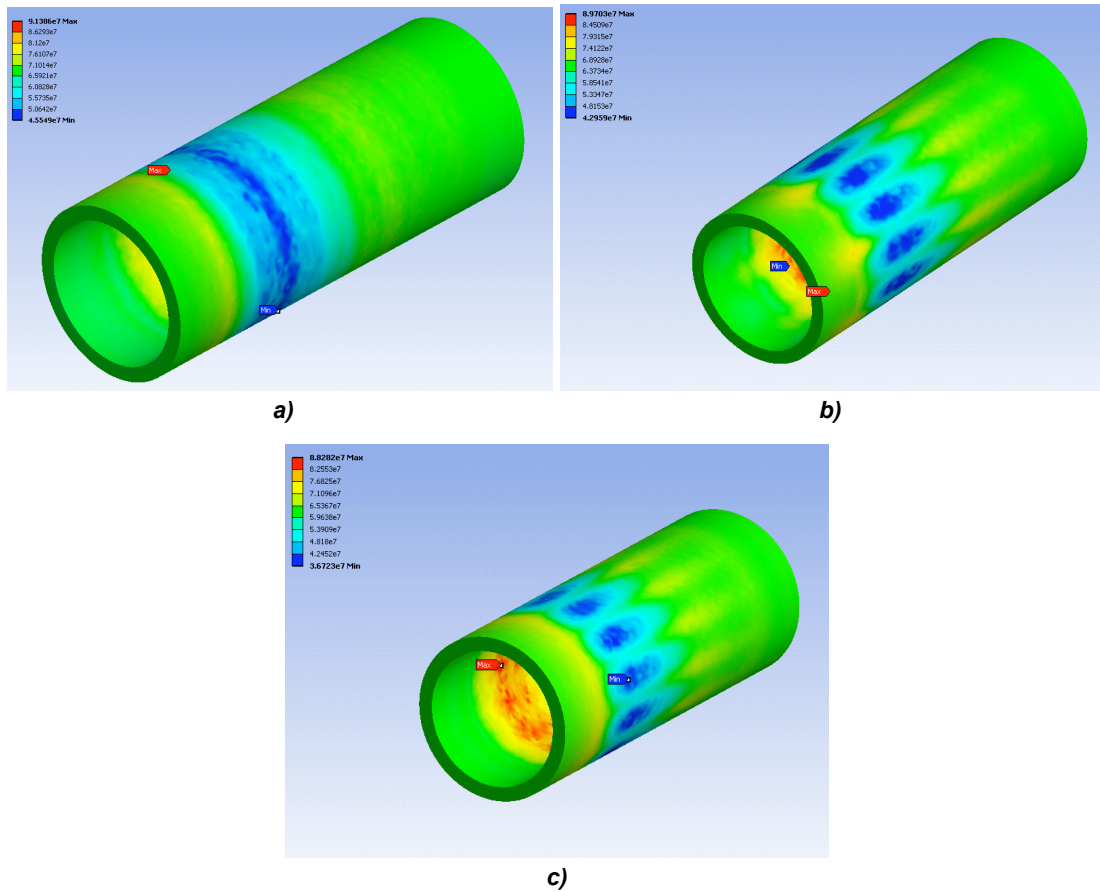
Figure 4: *Stress distribution for an AIN plasma chamber under vacuum and submitted to the cooling system pressure and to a non-uniform internal heat load of 6kW. a) helicoidal cooling circuit; b) race track; c) parallel channels.*

6 INITIAL ELECTROMAGNETIC STUDY OF THE LOSSES IN THE LINAC4 AND SPL PLASMA GENERATORS

It was aimed to develop an electromagnetic model of the Linac4 and SPL PGs to estimate power dissipation for thermal modelling. For the purposes of this initial study the Linac4 PG is simplified to three components (Fig. 5): the antenna, the ferrites and the NdFeB permanent magnets. The plasma is modelled as an egg shaped object in the centre of the antenna. OPERA from Vector Fields is used for the electromagnetic modelling.

Figure 5: The simplified model of the Linac4 plasma generator.

6.1 SKIN DEPTH

The skin depth δ provides an indication of where the eddy currents flow in the materials and hence where the ohmic heating losses are. The skin depth is calculated from the following equation:

$$\delta = \frac{1}{\sqrt{\pi f \mu_0 \mu_r \sigma}} \qquad (1)$$

where *f* is the frequency of the electromagnetic wave, μ_0 the magnetic constant, μ_0= 4π×10⁻⁷H/m, μ_R the relative permeability of the medium, and *σ* its electrical conductivity.

Table 4 shows the calculated skin depths for *f* = 2MHz. Nickel is shown because the NdFeB permanent magnets have a 10µm nickel coating to protect them from mechanical shocks. The skin depth calculation shows that most of the eddy current losses in the permanent magnets will be in the Nickel coating.

	NdFeB	Nickel	Copper	Ferrite
µᵣ (Typical)	500	250	1	1000
σ (Sm⁻)	6.67×10^5	1.40×10^7	6.0×10^7	1.0×10^{-5}
δ (µm)	19.4	6.02	45.9	3.56×10^6

Table 4: Skin depths δ calculated for the materials in the simplified source at f = 2MHz.

At 2MHz the skin depth in the ferrite is over 3.5m and therefore, much larger than the dimensions of the ferrite. For this reason, the eddy current loss calculation must include the entire volume of the ferrites.

6.2   ANTENNA PARAMETERS

The Linac 4 antenna has 5.5 turns with an inner radius of 30mm and 28.5mm winding length. The coil inductance in the presence of the ferrites was measured as 3.28µH. The coil resistance and the impedance at 2MHz were measured to be 0.23Ω and 41.2Ω, respectively. For 100kW rms power, the peak current I_{peak} and the peak voltage V_{peak} are 69.7A and 2870V, respectively. The average current and voltage I_{avg} and V_{avg} are 49.3A and 2030V, respectively.

6.3   MODELLING APPROACH

Accurate modelling of the currents flowing in the skin depth of the copper antenna and nickel coated NdFeB magnets in a time-varying non-linear simulation would require computing power and time beyond the scope of this initial study. Luckily several modelling shortcuts can be applied:

- The exact eddy currents in the antenna are not required. OPERA allows conductors to be modelled parametrically as Biot–Savart elements. These provide an acurrate representation of the fields produced outside the volume of the conductor.

- If ñ is a vector normal to the surface, the surface current density is given by ñ × H. As all of the current is flowing near the surface S, the average power dissipation P_{diss} over an ac cycle can be calculated by

$$P_{diss} = \frac{R_s}{2} \int_S H^2 dS \qquad (2)$$

where R_S is the surface resistance,

$$R_s = \frac{1}{\sigma \delta} \qquad (3)$$

Only the time varying component induces the eddy currents, so the permanent magnets are demagnetized in the model for the loss calculation in the nickel coating. The model is used to calculate the quasi-steady state integrals in equation (2) tangential to the nickel coated surface with the peak current applied to the antenna. Table 5 shows the calculated surface resistance for each of the materials at 2MHz.

	NdFeB	**Nickel**	**Copper**	**Ferrite**
R_s (Ω)	7.70×10^{-2}	1.19×10^{-2}	3.63×10^{-4}	NA

Table 5: *Calculated surface resistances R_S for the materials in the simplified source.*

To calculate the eddy current losses in the ferrites a non-linear time-varying solution can be easily performed because there is no need to model the very thin skin depth. The losses can then be calculated by integrating the current density squared and multiplying by the ferrite volume and resistivity.

6.4   SIMULATING THE PLASMA

The exact electromagnetic behavior of the plasma is very complicated and will change for different operation conditions. Thus the approach is to do a sweep of plasma permeability to see how that affects the losses in the other components.

Fig. 6 shows the magnetic fields in the model produced by the antenna at peak current. The field strength is significantly greater in the permanent magnets than the ferrites. The four magnets near the two gaps caused by the missing ferrites have stronger surface fields and hence higher losses. The calculated losses are shown in table 6 for different plasma permeabilities μ_P.
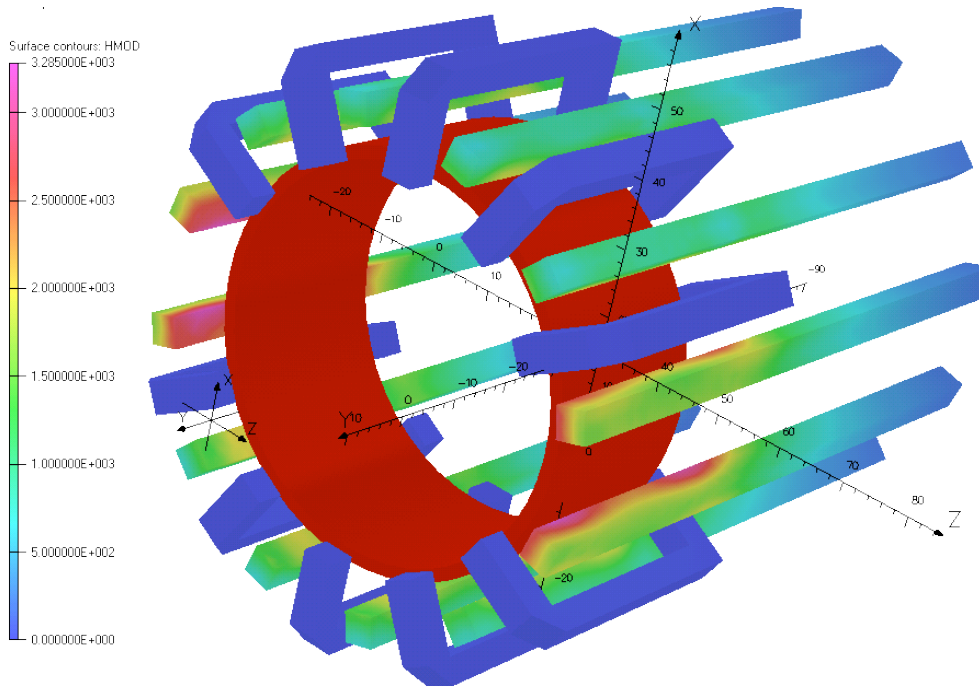

Figure 6: *The magnetic field in the model for a plasma with a relative permeability μ_P of 1000.*

μ_P	1	10	100	1000
Loss in Gap Magnets [W]	7.23	8.53	10.26	10.55
Loss in Other Magnets [W]	2.87	3.51	4.32	4.47
Total Loss in all Magnets [W]	51.88	62.16	75.62	77.93
Total Loss in all Ferrites [W]	0.95	1.27	1.58	1.62

Table 6: *Losses calculated for the magnets and ferrites for different plasma permeabilities μ_P.*

6.5 DISCUSSION

The results show that for an applied power of 100kW per ac cycle, the losses in the magnets and ferrites are very small and can reasonably be neglected in thermal modelling especially when the duty cycle of the source is taken into consideration. The nickel coating on the permanent magnets lowers the losses in the magnets by factor that is given by the ratio of surface resistances in table 5 ($\approx$ 6.5). Different plasma operating conditions could change the losses in the magnets and ferrites by up to 50%.

7 CONCLUSION AND OUTLOOK

The list of required improvements is established and the strategy to reach the nominal operation parameters is sketched. The demonstration of the scaling will be achieved by operating the Linac4 H$^-$ source with a pulsed and a constant gas injection and via measurements of double pulses at 20ms interval at a low repetition rate on the Linac4. Furthermore, the plasma of the Linac4 source and of the SPL plasma generator will be characterized by optical spectra. The coupling of the RF to the plasma will be measured. Additional tests of gas ignition and injection require the production of transparent mock-ups of the plasma chamber. Furthermore, it has been shown that electromagnetic losses in the cusp magnets and the ferrites that are very small and can reasonably be neglected in thermal modelling.

REFERENCES

[1] D. Küchler, T. Meinschad, J. Peters, R. Scrivens, A radio frequency driven H$^-$ source for Linac4. Rev. Sci. Instr. 79, 02A504 (2008)

[2] M. Baylac et al., Conceptual Design of the SPL II: A high-power superconducting H$^-$ linac at CERN. CERN-2006-006

[3] M. Kronberger, R. Scrivens, J. Lettry, Finite element thermal study of the Linac4 design source at the final duty factor. SLHC WP 7.1.1 Deliverable report, 03/2009

[4] R. F. Welton et al.: Next Generation H$^-$ Ion Sources for the SNS. AIP Conf. Proc. 1097, 181 (2009)